Research Article | Vol. 29, No. 16 / 2 August 2021 / Optics Express 24735
Optics EXPRESS

Check for updates

Experimental demonstration of pre-electronic dispersion compensation in IM/DD systems using an iterative algorithm

XIONG WU,[1] ABDULLAH S. KARAR,[2,*] KANGPING ZHONG,[3] ALAN PAK TAO LAU,[4,5] AND CHAO LU[1,5]

[1] *Photonics Research Center, Department of Electronic and Information Engineering, The Hong Kong Polytechnic University, Hong Kong, China*
[2] *College of Engineering and Technology, American University of the Middle East, Kuwait*
[3] *POET Technologies Inc, Shenzhen, China*
[4] *Photonics Research Center, Department of Electrical Engineering, The Hong Kong Polytechnic University, Hong Kong, China*
[5] *The Hong Kong Polytechnic University Shenzhen Research Institute, Shenzhen 518057, China*
[*] *abdullah.karar@aum.edu.kw*

Abstract: To combat chromatic dispersion (CD) in intensity modulation and direct detection (IM/DD) systems, three chirp-free demonstrations are experimentally performed with an iterative pre-electronic dispersion compensation (pre-EDC) algorithm at the transmitter end, for 28 GBaud non-return-to-zero on-off keying (NRZ-OOK), 56 GBaud NRZ-OOK and 28 GBaud four-level pulse-amplitude-modulation (PAM-4) signals, over distances of 100 km, 50 km and 40 km of single mode fiber (SMF), respectively. The iterative pre-EDC algorithm is based on the Gerchberg-Saxton (GS) algorithm, which treats the unconstrained phase at the direct detection receiver as a degree of freedom. At the receiver side, only a linear fractionally-spaced ($T/2$) post-feed-forward equalizer (post-FFE) is employed to combat the residual inter-symbol interference (ISI). Experimental results show that the aforementioned three demonstrations can approach the forward error correction (FEC) bit error rate (BER) threshold of 3.8×10^{-3} with (15 pre-EDC iterations and 5-tap post-FFE), (30 pre-EDC iterations and 15-tap post-FFE), and (10 pre-EDC iterations and 25-tap post-FFE), respectively. The results indicate the applicability of the pre-EDC algorithm in high-capacity IM/DD systems for transmission distances below 100 km of SMF.

© 2021 Optical Society of America under the terms of the OSA Open Access Publishing Agreement

1. Introduction

Long-haul coherent transceivers operating at a single channel enable data rates beyond 200 Gb/s and 400 Gb/s [1]. This forces metro, short-reach, and access networks to match these high modulation speeds, which are enabled by coherent transmission and detection. However, the cost associated with coherent technology in access and short-reach networks is prohibitive. The most feasible and cost effective solution is the use of intensity modulation and direct detection (IM/DD) [2]. The utilization of digital signal processing (DSP) [3], coupled with high speed digital-to-analog converters (DACs) [4–6], have enhanced the spectral efficiency (SE), data rates and reach of IM/DD systems. Despite the existence of a variety of advanced modulation techniques in IM/DD systems [7,8], the non-return-to-zero on-off keying (NRZ-OOK), and four-level pulse-amplitude modulation (PAM-4) [9], remains the most favorable for implementation in the extended reach 400 Gb/s Ethernet transmission [10].

Although IM/DD systems can employ a variety of transmitters, such as a Mach-Zehnder modulator (MZM), electro-absorption modulated laser (EML), or directly modulated laser (DML), they still exhibit high chromatic dispersion (CD), suffer power fading penalty and/or

#427661 https://doi.org/10.1364/OE.427661
Journal © 2021 Received 13 Apr 2021; revised 1 Jul 2021; accepted 9 Jul 2021; published 20 Jul 2021

Optics EXPRESS

chirp-induced nonlinear distortions when operating in the C-band [11]. Equalization algorithms to combat dispersion in IM/DD systems can be implemented at the transmitter [12] and/or receiver [9,13]. Such as, Volterra and Wiener equalizers [14], maximum likelihood sequence estimation based detection (MLSE) and its variants [15–17], vestigial-sideband modulation [18] and machine learning techniques [19]. However, algorithms for pre-electronic dispersion compensation (pre-EDC), which depend on fewer optical components, and eliminate the need for In-phase/Quadrature MZM modulators or single sideband filters, offer lower cost, complexity and are amenable to implementation in short-reach IM/DD systems.

Recently, a novel EDC algorithm for IM/DD systems employing a single drive MZM transmitter was proposed [20–22]. Initially, the Gerchberg-Saxton (GS) algorithm [23–25] is adopted for dispersion pre-compensation through utilizing the link dispersion for time-to-frequency mapping [26,27], while imposing appropriate constraints on the amplitude and phase of the optical signal at both the output of the transmitter and prior to the direct detection receiver [22]. The resulting iterative algorithm can be used to pre-compensate for dispersion at the transmitter using amplitude-only control of a chirp-free MZM, while treating the unconstrained phase at the direct detection receiver as a degree of freedom. This pre-EDC with the temporally iterative amplitude constraints can be regarded as a CD-oriented pre-emphasis around the CD-induced frequency nulls in the frequency domain. As for other common approaches, such as receiver-side Volterra based nonlinear equalizers (VNLE) and MLSE, they directly deal with the CD-induced nonlinear inter-symbol interference (ISI) using high order terms. This is achieved with a high number of VNLE taps or high number of MLSE states to accommodate a longer memory length, both posing huge complexity in high speed IM/DD systems. Some of the notable results utilizing these algorithms are 56 GBaud PAM-4 over 7.5 km of single mode fiber (SMF) [15], 28 GBaud PAM-4 over 30 km of SMF [16], 56 GBaud OOK over 70 km of SMF [17], under the forward error correction (FEC) bit error rate (BER) threshold of 3.8×10^{-3}. In this work, this iterative dispersion pre-compensation algorithm is experimentally demonstrated for IM/DD transmission links at 28 GBaud NRZ-OOK over 100 km of SMF, 56 GBaud NRZ-OOK over 50 km of SMF, and 28 GBaud PAM-4 over 40 km of SMF, under 3.8×10^{-3} BER threshold. Furthermore, the effect of baud rate, pulse shaping roll-off factor (RoF), digital extinction ratio (ER), and the number of pre-EDC iterations are also investigated.

This paper is organized as follows. In section 2, the experimental setup and the utilized DSP algorithm are described; in section 3, the measurement results are presented for both NRZ-OOK and PAM-4, while the paper is concluded in section 4.

2. Experimental set-up

The experimental setup used in this work is shown in Fig. 1, which highlights three complementary parts: the schematic diagram of the iterative pre-EDC processing at the digital transmitter, the SMF transmission link, and the DSP processing at the receiver.

In the first part, $s'^{(0)}(t)$ in the digital transmitter is initially set to $s^{(0)}(t)$, the temporal amplitude of the ideal pulse-shaped OOK/PAM-4 ($P(t)$) signals by a raised-cosine (RC) filter with certain digital ER and a pre-defined RoF. Digital ER is defined as the ratio (dB) between the highest and the lowest power level of digital $P(t)$. Both digital ER and RoF contribute to the temporal amplitude of signals. At the n^{th} iteration of the pre-EDC, $s^{(n)}(t) = |s'^{(n-1)}(t)|$ in the transmitter is digitally propagated through a SMF link with chromatic dispersion coefficient $+D$ and resulting in $r^{(n)}(t) = |r^{(n)}(t)|e^{j\measuredangle r^{(n)}(t)}$ in the digital receiver. Subsequently, the receiver constraints are imposed converting $|r^{(n)}(t)|$ to $|s^{(0)}(t)|$. Then the amplitude-constrained $r'^{(n)}(t) = |s^{(0)}(t)|e^{j\measuredangle r^{(n)}(t)}$ with the unconstrained phase $\measuredangle r^{(n)}(t)$ is digitally re-transmitted through the same-length SMF link with $-D$ coefficient. Consequently, at the digital transmitter side, the received complex signal is $s'^{(n)}(t)$. The transmitter side constraints dictate that the phase of $s'^{(n)}(t)$ is removed, while the transmitted amplitude signals are updated for the next iterative transmission. After N iterations, the received

Optics EXPRESS

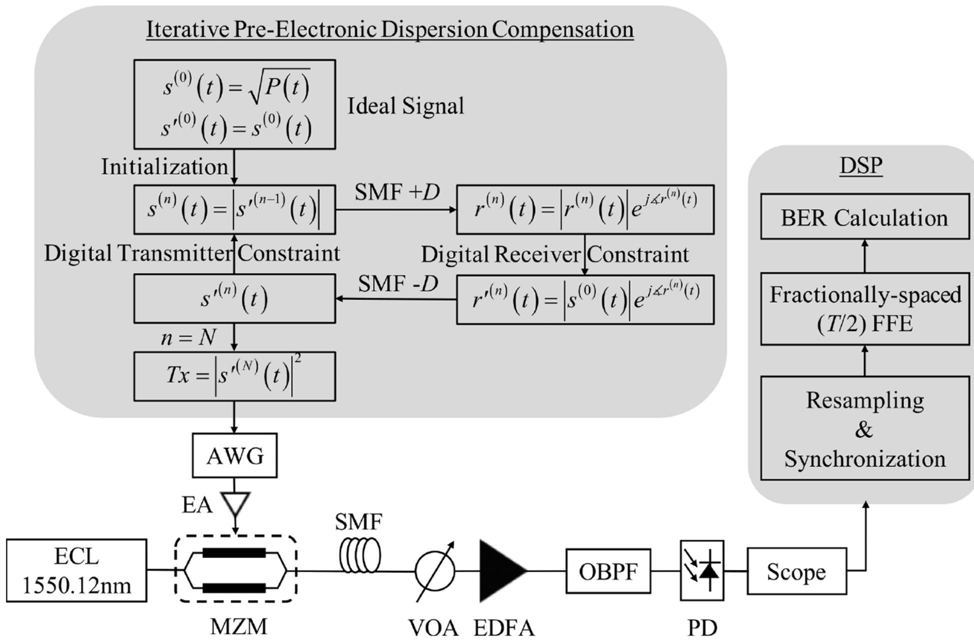

Fig. 1. Experimental set-up. AWG: Arbitrary waveform generator; EA: Electrical amplifier; MZM: Mach–Zehnder Modulator; ECL: External cavity laser; SMF: Single mode fiber; VOA: Variable optical attenuator; EDFA: Erbium-Doped Fiber Amplifier; OBPF: Optical bandpass filter; PD: Photodetector; DSP: Digital signal processing; FFE: Feed-forward equalizer.

$|r^{(n)}(t)|$ signal intensity profile will approach the intensity profile of $|s^{(0)}(t)|$, namely the ideal temporal amplitude of NRZ-OOK/PAM-4. To that end, the pre-EDCed $|s'^{(N)}(t)|^2$ is ready for the arbitrary waveform generator (AWG, *Keysight* M8194A, 120 GSa/s) with integer sampling. In this work, 28 GBaud NRZ-OOK, 56 GBaud NRZ-OOK and 28 GBaud PAM-4 are implemented, using a 2^{17} pseudo random binary sequences (PRBS). Furthermore, different digital ERs and different RoFs of RC filter are taken into account for the practical verification of the pre-EDC.

In the second part, the output of the AWG is electrically amplified and used to drive a chirp-free single-drive MZM (*Fujitsu* FTM7938EZ, ~32 GHz) biased at the quadrature point. The optimal optical ER is determined by the transmitter set-up under back-to-back conditions, to ensure the MZM operates in the linear region. This is achieved through optimizing the magnitude of the AWG's output and the MZM bias point, and through the analysis of the back-to-back eye-opening factor. To facilitate a fair comparison, all transmitter parameters were optimized according to the back-to-back case as opposed to for each pre-distortion. The set-up utilizes an external cavity laser (ECL) operating at 1550.12 nm. After SMF transmission (100 km for 28 Gbaud NRZ-OOK, 50 km for 56 GBaud NRZ-OOK and 40 km for 28 GBaud PAM-4, respectively with 16.8, 16.8 and 16.3 ps/nm/km dispersion coefficient), the received optical signals are attenuated by a variable optical attenuator (VOA) to adjust the received optical power (ROP). An erbium-doped fiber amplifier (EDFA) along with a 0.8 nm optical bandpass filter (OBPF) is placed prior to the direct detection, which is achieved with a ~50GHz photodetector (PD). The electrical waveform is then collected by the real-time sampling oscilloscope (*Keysight* DSAZ634A Infiniium Oscilloscope, 160 GSa/s).

In the third part, the received signals undergo a sequence of DSP steps: resampling, synchronization, fractionally-spaced ($T/2$) feed-forward equalizer (FFE) and BER calculation. It is worth noting that the simple $T/2$ FFE is only used for timing phase offset compensation and linear equalization simultaneously.

3. Results and discussion

3.1. NRZ-OOK at 28 GBaud over 100 km SMF

The measured BER at different ERs (0.5 dB, 1 dB, 2 dB, 3 dB and 6 dB) for the 28 GBaud NRZ-OOK with RoF of 1 over 100 km SMF versus the number of pre-EDC iterations at a maximum ROP of −16.9 dBm and 5-tap post-FFE is shown in Fig. 2. It is evident that the optimum digital ER is around 2 dB, whereas the benefit of increasing the number of pre-EDC iterations is reduced beyond 15 iterations. This is expected as the original GS algorithm obtains an optimal solution invariant to transformations between time and frequency domains and converges within the first few iterations [25]. Any additional algorithm executions would have little effect on the reached optimum. A detailed analysis of pre-EDC convergence will be presented in subsection 3.4.

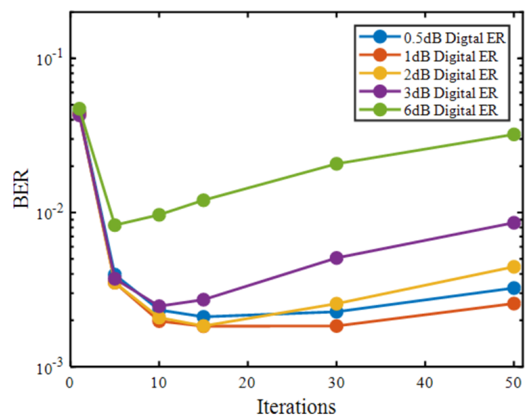

Fig. 2. NRZ-OOK at 28 GBaud over 100 km SMF: BER versus number of iterations after pre-EDC with different digital ERs under 5-tap post-FFE, at maximum ROP of −16.9 dBm.

Hence the digital ER is set to 2 dB, and the number of pre-EDC iterations is set to 15. To investigate the effect of the number of post-FFE taps on the system performance, Fig. 3(a) shows the BER versus different ROPs from −27.9 dBm to −16.9 dBm with different number of taps (3, 5 and 15 taps) for the post-FFE with and without the pre-EDC. It is observed that only utilizing the post-FFE at the receiver cannot recover the transmitted data, without the essential benefit of the pre-EDC algorithm at the transmitter end. Admittedly, utilization of 15-tap post-FFE improves the BER performance compared to 3-tap and 5-tap cases. However, the resulting BERs are far higher than the FEC BER threshold of 3.8×10^{-3}, rendering the system inoperable in practical settings. However, by implementing both the pre-EDC and post-FFE, the BER is improved and falls below the FEC threshold. Undoubtedly, the BER performance is better with more taps for the post-FFE which compensate longer ISI among adjacent symbols. Furthermore, there is a marginal BER improvement with 15-tap post-FFE in comparison to the BER with 5-tap post-FFE, which indicates there is insignificant ISI when pre-EDC is present. As a trade-off between the BER performance and post-FFE's complexity, utilization of 5-tap post-FFE is sufficient for this experimental demonstration. The FEC threshold is reached at a −21 dBm ROP. The improvement of pre-EDC can be directly observed from the electrical frequency spectra and electrical eye-diagrams of the received signals at maximum ROP of −16.9 dBm in Figs. 3(b) to 3(e), respectively. Without pre-EDC, there is CD-induced frequency power fading of the spectrum in Fig. 3(b) and unrecognized eye-diagram in Fig. 3(d). With the help of pre-EDC, the spectrum is much emphasized near the fading frequencies in Fig. 3(c) and the eye-diagram in Fig. 3(e) is quite clear showing that the residual ISI is small.

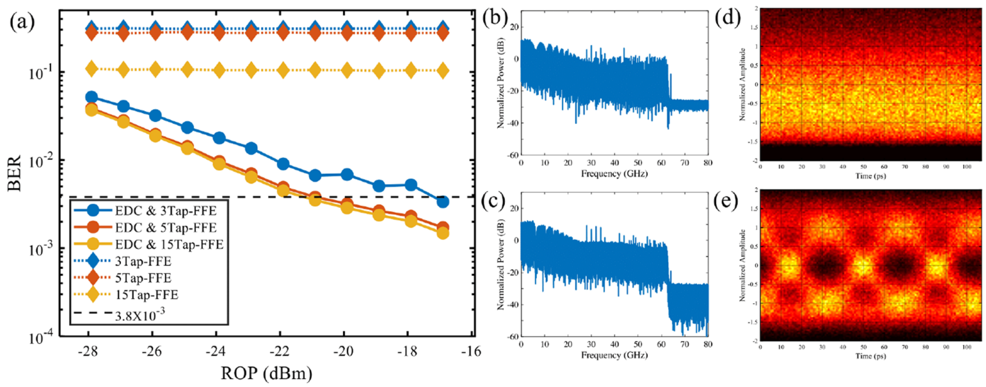

Fig. 3. NRZ-OOK at 28 GBaud over 100 km SMF: (a) BER versus ROP (−27.9 dBm to −16.9 dBm) with different taps for post-FFE, under no pre-EDC and pre-EDC with 2 dB digital ER and 15 iterations. Frequency spectra of received signals at maximum ROP of −16.9 dBm under: (b) no pre-EDC and (c) pre-EDC. Eye-diagrams of received signals at maximum ROP of −16.9 dBm under: (d) no pre-EDC and (e) pre-EDC.

Furthermore, the effect of different RoFs ranging from 0 to 1 of the RC filter on the BER is considered and the corresponding results are shown in Fig. 4, at a ROP of −16.9 dBm, 2 dB digital ER, 15 pre-EDC iterations and 5-tap post-FFE. It is evident that the optimal BER is reached at the RoF of 1. Reducing the RoF degrades the BER performance, while a RoF exceeding 0.5 can still result in a BER below the FEC BER threshold of 3.8×10^{-3}.

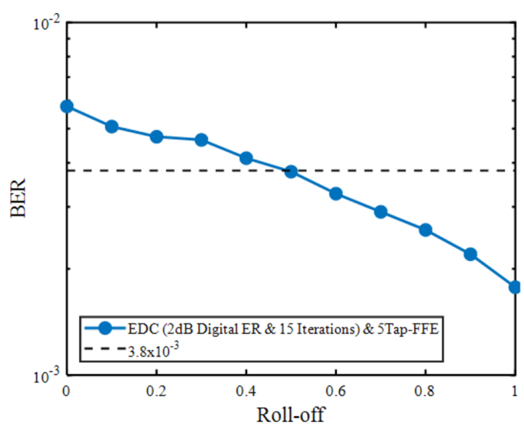

Fig. 4. NRZ-OOK at 28 GBaud over 100 km SMF: BER versus different RoFs (0 to 1) of RC filter under pre-EDC with 2dB digital ER and 15 iterations and under 5-tap post-FFE, at maximum ROP of −16.9 dBm.

For a more comprehensive analysis of the pre-EDC, the effect of the combination of baud rate (ranging from 14 GBaud to 56 GBaud) and number of iterations (ranging from 0 to 200 iterations) is also investigated both in simulation and experiment. In the simulation with only CD effect considered (without any additive white Gaussian noise, AWGN), the simulated BER versus different combinations is shown in Fig. 5(a), at 1 RoF, 2 dB digital ER and 5-tap post-FFE.

It is observed that there are different saturated iteration numbers satisfying BER $<10^{-6}$ for the corresponding tested baud rate. Evidently, all saturated iterations are lower than 50 and a few are lower than 20. Furthermore, the experimental results are shown in Fig. 5(b), at a ROP of −16.9 dBm and with the remaining parameters matching those in the simulation. Different baud rate can find its corresponding optimal iteration number rather than the saturated value, which is mainly limited by the practical factors and will be discussed in subsection 3.4. From the experimental results, the optimal iteration number is slightly higher as the baud rate increases, which is still in an acceptable range compared to other iterative algorithms with up to hundreds of iterations. Besides, the maximum baud rate of NRZ-OOK over 100 km SMF transmission can be slightly extended from 28 GBaud to around 30 GBaud with the corresponding optimal iteration within the FEC threshold.

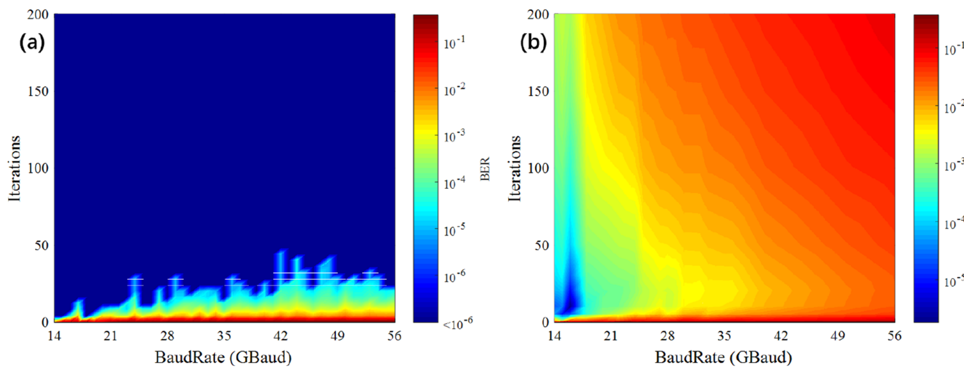

Fig. 5. NRZ-OOK over 100 km SMF: (a) Simulated BER versus different combinations of iteration and baud rate of pre-EDC (2dB digital ER) under 5-tap post-FFE, without any AWGN. (b) Experimental BER versus different combinations of iteration and baud rate of pre-EDC (2 dB digital ER) under 5-tap post-FFE, at maximum ROP of −16.9 dBm.

Based on all aforementioned results for the 28 GBaud NRZ-OOK signals over 100 km SMF transmission, the proposed pre-EDC algorithm is feasible with a small number of iterations and certain bandwidth tolerance in practical IM/DD systems.

3.2. NRZ-OOK at 56 GBaud over 50 km SMF

With the same capacity–distance product of 2.8 Tb/s · km, the 56 GBaud NRZ-OOK over 50 km SMF implemented with the pre-EDC is demonstrated and investigated in this subsection. The measured BER at different ERs (0.5 dB, 1 dB, 2 dB, 3 dB, and 6 dB) versus the number of pre-EDC iterations at a maximum ROP of −6.8 dBm and 15-tap post-FFE is shown in Fig. 6. At 1 dB digital ER, the resulting BER outperforms the BER at other digital ERs within the same number of iterations. Evidently, the optimal digital ER and optimal number of iterations are 1 dB and 30 iterations, respectively.

Furthermore, the effect of the number of post-FFE taps (5, 15, and 25 taps) on BER is also investigated at different ROPs from −21.8 dBm to −6.8 dBm, with and without the pre-EDC at 1 dB digital ER and 30 iterations. The corresponding BERs are shown in Fig. 7(a). With 5-tap post-FFE, the BER with pre-EDC at all tested ROPs cannot reach the FEC threshold of BER = 3.8×10^{-3}. However, with the 15-tap post-FFE and with 25-tap post-FFE, their BERs can reach the FEC threshold at around −15 dBm ROP, and both achieve the similar performance versus different ROPs. This indicates that with the pre-EDC the BER performance is saturated with 15-tap post-FFE, which indicates the existence of a marginal amount of ISI. It is evident that the pre-EDC is essential as the system becomes inoperable with a BER higher than 1×10^{-1} at all tested taps and all ROPs. In Figs. 7(b) and 7(c), the electrical frequency spectra of the received

Optics EXPRESS

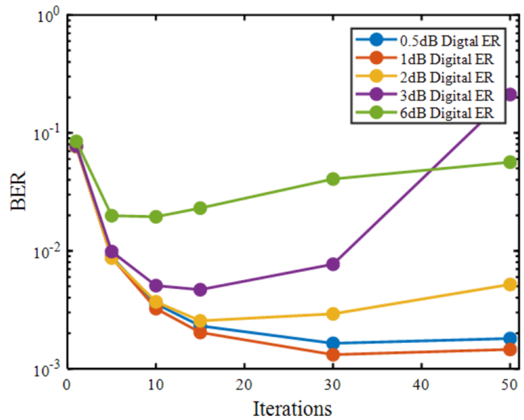

Fig. 6. NRZ-OOK at 56 GBaud over 50 km SMF: BER versus iteration after pre-EDC with different digital ERs under 15-tap post-FFE, at maximum ROP of −6.8 dBm.

signals at −6.8 dBm ROP without and with pre-EDC are illustrated, respectively. In addition, the electrical eye-diagrams of the received signal at −6.8 dBm ROP without and with pre-EDC are illustrated in Figs. 7(d) and 7(e), respectively. The pre-EDC is essential for dispersion compensation as a pre-emphasized frequency spectrum and an acceptable eye-diagram for the 56 GBaud NRZ-OOK signals over 50 km SMF transmission appears. However, the received eye-diagram is poor in comparison to the eye-diagram of 28 GBaud NRZ-OOK over 100 km transmission in Fig. 3(e).

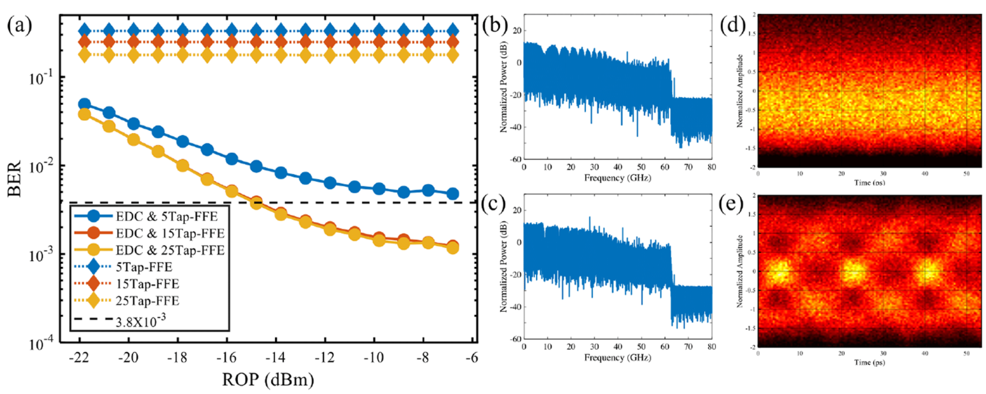

Fig. 7. NRZ-OOK at 56 GBaud over 50 km SMF: (a) BER versus ROP (−21.8 dBm to −6.8 dBm) with different taps for post-FFE, under no pre-EDC and pre-EDC with 1dB digital ER and 30 iterations. Frequency spectra of received signals at maximum ROP of −6.8 dBm under: (b) no pre-EDC and (c) pre-EDC. Eye-diagrams of received signals at maximum ROP of −6.8 dBm under: (d) no pre-EDC and (e) pre-EDC, at maximum ROP.

Furthermore, at a ROP of −6.8 dBm and with the above optimal parameters of the pre-EDC along with 15-tap post-FFE, the effect of different RoFs from 0 to 1 of the RC filter is investigated and the corresponding results are shown in Fig. 8. Remarkably, the BERs at all RoFs are lower than 2.2×10^{-3} with a certain margin referred to the FEC threshold and BER at the RoF of 1 is the optimal one. The fluctuation is also observed when RoF is near 0.

Although this demonstration with the pre-EDC of 56 GBaud NRZ-OOK over 50 km SMF requires double pre-EDC iterations and triple post-FFE taps in comparison to the 28 GBaud

Optics EXPRESS

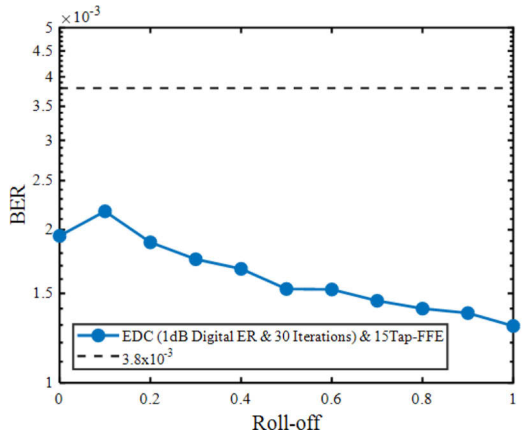

Fig. 8. NRZ-OOK at 56 GBaud over 50 km SMF: BER versus different RoFs (0 to 1) of RC filter under pre-EDC with 1dB digital ER and 30 iterations and under 15-tap post-FFE, at maximum ROP of −6.8 dBm.

NRZ-OOK over 100 km SMF, these results still verify the robustness of the pre-EDC algorithm practically applied with high baud rate NRZ-OOK signals in such IM/DD systems.

3.3. PAM-4 at 28 GBaud over 40 km SMF

In this subsection, the results of the pre-EDC of 28 GBaud PAM-4 over 40 km SMF are presented and analyzed. The measured BER at different digital ERs (0.5 dB, 1 dB, 2 dB, 3 dB and 6 dB) versus the number of EDC iterations at a maximum ROP of −9.3 dBm and 25-tap post-FFE is shown in Fig. 9. Evidently, the optimal BER can be found at 2 dB digital ER and 10 iterations.

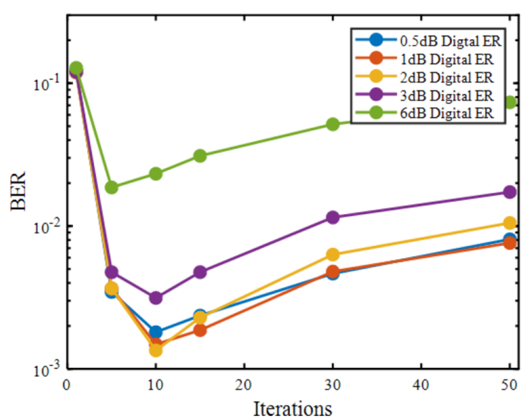

Fig. 9. PAM-4 at 28 GBaud over 40 km SMF: BER versus iteration after pre-EDC with different digital ERs under 25-tap post-FFE, at maximum ROP of −9.3 dBm.

The results in Fig. 10(a), show the BER versus different ROPs, while changing the number of taps (15, 25, and 35 taps) for the fractionally-spaced post-FFE with and without pre-EDC under a 2 dB digital ER and 10 iterations. The electrical frequency spectra and eye-diagrams of the received 28 GBaud PAM-4 signals at maximum ROP of −9.3 dBm without pre-EDC and with pre-EDC are shown in Figs. 10(b) to 10(e), respectively. Although different from the results of 28 GBaud and 56 GBaud NRZ-OOK respectively in Fig. 3(a) and Fig. 7(a), in relation to the saturated BER performance (5-tap and 15-tap post-FFE), here the BER with the pre-EDC versus

Optics EXPRESS

different ROPs from −20.3 dBm to −9.3 dBm does not reach saturation when taps are from 25 to 35. At the ROP of −9.3 dBm, the BER is decreased from 1.3×10^{-3} to 4.7×10^{-4}, when the taps are increased from 25 to 35. These results show that there is strong ISI. The effect of this ISI can be found through the distorted electrical eye-diagram of the received 28 GBaud PAM-4 signals in Fig. 10(e). However, with the utilization of 25-tap post-FFE, the BER performance is within the FEC threshold, which can be achieved at around −14 dBm ROP. Nevertheless, without the pre-EDC, the electrical eye-diagram of 28 GBaud PAM-4 in Fig. 10(d) is indistinguishable and BERs are higher than 2×10^{-2} at all tested taps for the post-FFE and at all tested ROPs in Fig. 10(a).

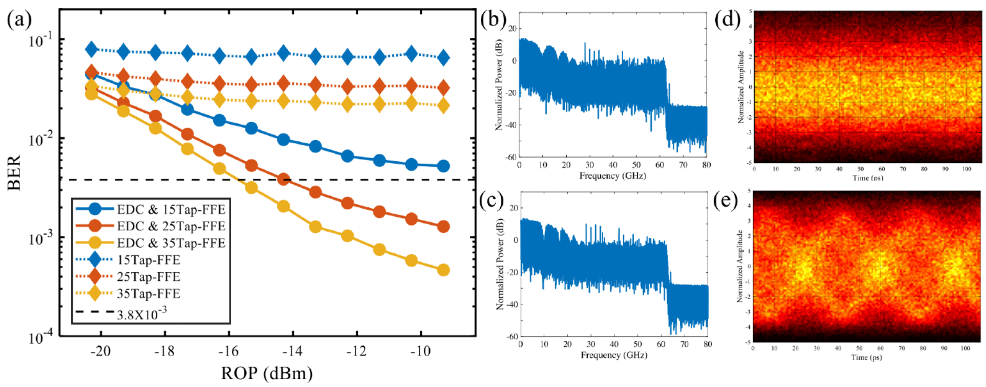

Fig. 10. PAM-4 at 28 GBaud over 40 km SMF: (a) BER versus ROP (−20.3 dBm to −9.3 dBm) with different taps of post-FFE, under no pre-EDC and pre-EDC with 2dB digital ER and 10 iterations. Frequency spectra of received signals at maximum ROP of −9.3 dBm under: (b) no pre-EDC and (c) pre-EDC. Eye-diagrams of received signals at maximum ROP of −9.3 dBm under: (d) no pre-EDC and (e) pre-EDC.

The effect of different RoFs from 0 to 1 of the RC filter on the BER is also investigated and results are shown in Fig. 11, at a ROP of −9.3 dBm, 2 dB digital ER, 10 pre-EDC iterations and 25-tap post-FFE. When the RoF of RC filter is 1, the optimal BER is achieved at around 1.3×10^{-3}. Evidently, the BER performance is severely degraded with the decrease of RoF. When the RoF is less than 0.8, the corresponding BERs are higher than 3.8×10^{-3}.

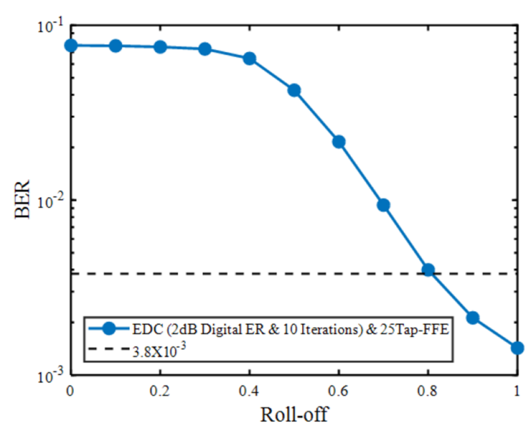

Fig. 11. PAM-4 at 28 GBaud over 40 km SMF: BER versus different RoFs (0 to 1) of RC filter under pre-EDC with 2dB digital ER and 10 iterations and under 25-tap post-FFE, at maximum ROP of −9.3 dBm.

Optics EXPRESS

In Figs. 12(a) and 12(b), the BER versus different combinations of baud rate (ranging from 14 GBaud to 56 GBaud) of PAM-4 over 40 km SMF transmission and number of iterations (ranging from 0 to 200 iterations) of simulation and experiment are shown, respectively. In Fig. 12(a), the simulated results are presented with only CD effect considered. Unlike the 28 GBaud NRZ-OOK results in Fig. 5(a), with 200 iterations there are still several combinations for PAM-4, with BERs higher than 3.8×10^{-3}. In the area near 28 GBaud with iterations less than 25, the BER can be lower than 1×10^{-6}. This area can also be found in the experimental results in Fig. 5(b) with BER around 1×10^{-3}, at a ROP of −9.3 dBm, 2 dB digital ER, 1 RoF and 25-tap post-FFE. When the baud rate is increased beyond this region, the system works poorly with BER higher than 3.8×10^{-3}. At a lower baud rate less than 20 GBaud, the corresponding BER is acceptable with few iterations or even without iterations (no pre-EDC) for certain baud rates.

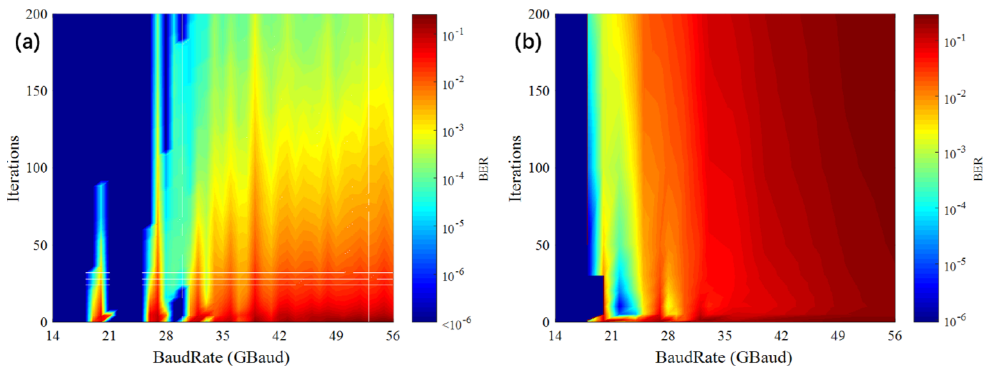

Fig. 12. PAM-4 over 40 km SMF: (a) Simulated BER versus different combinations of iteration and baud rate of pre-EDC (2 dB digital ER) under 25-tap post-FFE, without any AWGN. (b) Experimental BER versus different combination of iteration and baud rate of pre-EDC (2 dB digital ER) under 25-tap post-FFE, at maximum ROP of −9.3 dBm.

With the benefit of the pre-EDC algorithm and the post-FFE, this 28 GBaud PAM-4 over 40 km SMF demonstration occupies a capacity–distance product of 2.24 Tb/s · km. This demonstration indeed indicates that the pre-EDC has a great potential in IM/DD systems with high baud rate and high spectral-efficient modulation formats over tens of kilometers of SMF.

3.4. Pre-EDC convergence and amplitude distributions

For the convergence of pre-EDC, the digital ER is a key factor. It can be guaranteed to converge theoretically with a small digital ER based on the small-signal analysis (referring to small modulation index or small digital ER) [28]. As for a large ER, the convergence expression is not always guaranteed with a closed-form solution. Below presents the proof using frequency domain analysis. The following matrix equation relates the intensity modulation (IM) and phase modulation (PM) of fiber CD frequency domain transfer function based on small-signal analysis:

$$\begin{bmatrix} \Delta S_{out} \\ \varphi_{out} \end{bmatrix} = \begin{bmatrix} \cos(\theta) & -2P_0 \sin(\theta) \\ \frac{\sin(\theta)}{2P_0} & \cos(\theta) \end{bmatrix} \begin{bmatrix} \Delta S_{in} \\ \varphi_{in} \end{bmatrix}, \tag{1}$$

$$\theta = \frac{D\lambda^2\omega^2 L}{4\pi c}, \tag{2}$$

where θ is the CD-induced phase shift in the frequency domain, D is the CD coefficient, λ is the wavelength, ω is the frequency of modulated signal, L is the fiber length, and c is the light speed; P_0 is the average power of the optical signal, ΔS_{in}, ΔS_{out}, φ_{in}, and φ_{out} are the frequency responses

Optics EXPRESS

of the input signal intensity, output signal intensity, input signal phase, and output signal phase, respectively. It is worth noting that the ΔS_{in} and ΔS_{out} are assumed to be alternating-current (AC) coupled, with the large P_0 removed.

The following walks-though the iterative algorithm. Propagation with CD of $+\theta$ ($+D$) in the 1^{st} iteration:

$$\begin{bmatrix} \Delta S_R^1 \\ \varphi_R^1 \end{bmatrix} = \begin{bmatrix} \cos(\theta) & -2P_0 \sin(\theta) \\ \frac{\sin(\theta)}{2P_0} & \cos(\theta) \end{bmatrix} \begin{bmatrix} \Delta S_{ideal} \\ 0 \end{bmatrix}, \tag{3}$$

$$\varphi_R^1 = \frac{\sin(\theta)}{2P_0} \Delta S_{ideal}, \tag{4}$$

where ΔS_R^1, φ_R^1 are the intensity and phase responses at the digital receiver; ΔS_{ideal} is the transmitted ideal intensity response.

Back-propagation with $-D$ at the 1^{st} iteration (amplitude constraint and phase unconstrained at the digital receiver, using the ideal amplitude ΔS_{ideal} to replace the received ΔS_R^1):

$$\begin{bmatrix} \Delta S_T^1 \\ \varphi_T^1 \end{bmatrix} = \begin{bmatrix} \cos(\theta) & 2P_0 \sin(\theta) \\ -\frac{\sin(\theta)}{2P_0} & \cos(\theta) \end{bmatrix} \begin{bmatrix} \Delta S_{ideal} \\ \varphi_R^1 \end{bmatrix}, \tag{5}$$

substituting Eq. (4) into Eq. (5), the required pre-distorted small-signal intensity response ΔS_T^1 at the transmitter after the 1^{st} iteration can be expressed as:

$$\Delta S_T^1 = \left[\cos(\theta) + \sin^2(\theta)\right] \Delta S_{ideal}. \tag{6}$$

When the forward and backward propagation are imparted for the 2^{nd} iteration, the received phase response φ_R^2 and the required pre-distorted intensity response ΔS_T^2 at the transmitter are:

$$\varphi_R^2 = \frac{\sin(\theta)}{2P_0} \left[\cos(\theta) + \sin^2(\theta)\right] \Delta S_{ideal}, \tag{7}$$

$$\Delta S_T^2 = \left[\cos(\theta) + \sin^2(\theta) \left[\cos(\theta) + \sin^2(\theta)\right]\right] \Delta S_{ideal}. \tag{8}$$

We can deduce that at the N^{th} iteration:

$$\Delta S_T^N = \cos(\theta) S_{ideal} + \sin^2(\theta) \Delta S_T^{N-1}, \tag{9}$$

$$\Delta S_T^N = \left[\cos(\theta) + \sin^2(\theta) \left[\cos(\theta) + \sin^2(\theta) [\ldots]\right]\right] \Delta S_{ideal}. \tag{10}$$

Consequently, the final received signal is given by the following recursive expression:

$$\Delta S_R = \cos(\theta) \left[\cos(\theta) + \sin^2(\theta) \left[\cos(\theta) + \sin^2(\theta) [\ldots]\right]\right] \Delta S_{ideal}. \tag{11}$$

At a small enough digital ER and with a certain number of iterations, the pre-EDC algorithm will converge $\left[\cos(\theta) + \sin^2(\theta) \left[\cos(\theta) + \sin^2(\theta) [\ldots]\right]\right]$ to closely approximate $1/\cos(\theta)$, with an unbounded value at the frequency fading notches and bounded value at their vicinity, as shown in Fig. 13(a). As the number of iterations increases, ΔS_R will converge to closely match ΔS_{ideal}, while sharpening the frequency notches. Equivalently, ΔS_T^N will exhibit a larger lifting around these frequency notches as shown in Fig. 13(b). In return more electrical quantization noise will be posed by the resolution-limited DAC in time domain [29].

At a large digital ER, the small-signal analysis cannot be effectively applied, and the convergence may not be guaranteed with a numerical calculation. In Fig. 14, the simulated BERs are depicted for the aforementioned three experimental cases with different digital ERs (0.5 dB to 10 dB). All

Optics EXPRESS

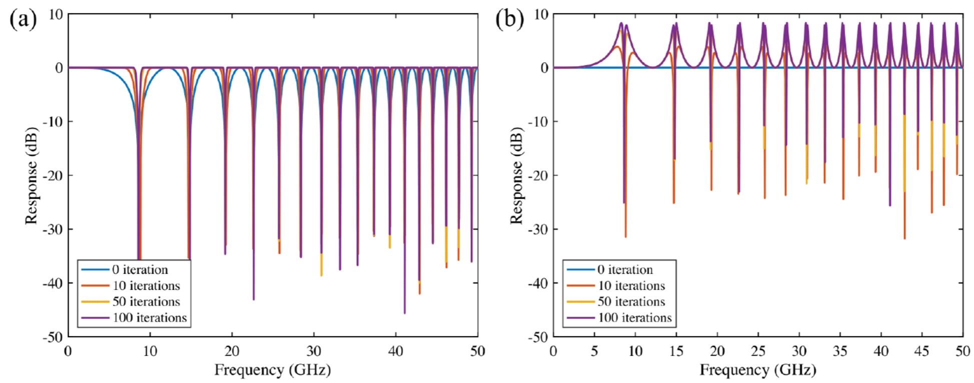

Fig. 13. Response versus frequency at 17 ps/nm/km under at 50 km SMF transmission: (a) $\Delta S_R/\Delta S_{ideal}$, (b) $\Delta S_T^N/\Delta S_{ideal}$.

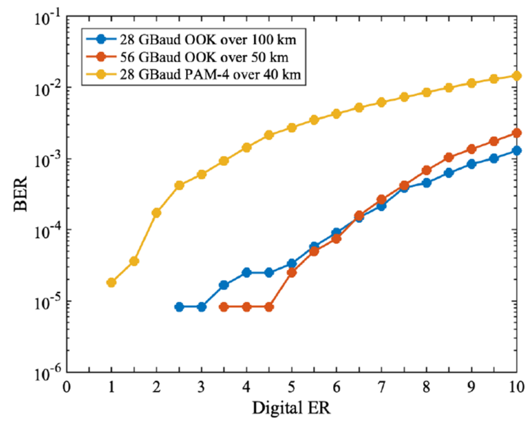

Fig. 14. BER versus different digital ERs under three cases without AWGN: (28 GBaud NRZ-OOK over 100 km, 56 GBaud NRZ-OOK over 50 km, and 28 GBaud PAM-4 over 40 km).

parameters for pre-EDC and FFE are set according to experiments presented in earlier subsections and no AWGN exists.

For the issue of practical implementation, it has not been fully considered yet. In this work, the iterative process is conducted using Matlab and the fiber model is handled in the frequency domain with the fast Fourier transform (FFT) and inverse FFT (iFFT) operations. As a consequence, the complexity of the proposed pre-EDC will be a concern and a drawback in practice, compared to other non-iterative received-based DSP schemes. Further work is needed to speed up the algorithm convergence and realizes an efficient digital fiber model with adjustable parameters reducing the complexity.

In the following analysis, the transmitted amplitude distributions with the pre-EDC are also investigated. The amplitude distributions versus different combinations of digital ER (0.5 dB, 1 dB, 2 dB, 3 dB and 6 dB) and iterations (1, 10, 30, 100 and 200) of 28 GBaud NRZ-OOK for 100 km SMF, 56 GBaud NRZ-OOK for 50 km SMF and 28 GBaud PAM-4 for 40 km SMF, are shown in Figs. 13(a), 13(b) and 13(c), respectively. Here the distribution is centered (mean removed) and normalized from -1 to 1, meeting the requirements of AWG and its following EA with direct-current (DC) block in Fig. 1.

Optics EXPRESS

It is observed that at 0.5 dB and 1 dB digital ER, the corresponding amplitude distributions always maintain a Gaussian shape with 1 to 200 iterations. However, with more iterations where the convergence is guaranteed, more power is concentrated at the center, which induces quantization noise by the DAC. Hence an excess of iterations would pose a negative effect on BER in real transmission. This can be shown from BERs of the experimental results in subsection 3.1, 3.2 and 3.3. Furthermore, at a large digital ER of 6 dB all corresponding amplitudes are severely distorted. As for NRZ-OOK signals at 2 dB and 3 dB digital ER in Figs. 15(a) and 15(b), they both have the amplitude aggregation and one-side distribution problem when exposed to a large number of iterations. While for PAM-4 signals at 2 dB and 3 dB digital ER in Fig. 15(c), the distributions are similar to those at smaller digital ER when the iteration is less than 100. This similarity is also reflected in BERs in Fig. 9 where the four corresponding BER curves are close. As such when implementing the proposed pre-EDC algorithm in a particular IM/DD system to combat CD, the parameters are essential and the practical trade-off and balance between the digital ER and number of iteration needs to be determined.

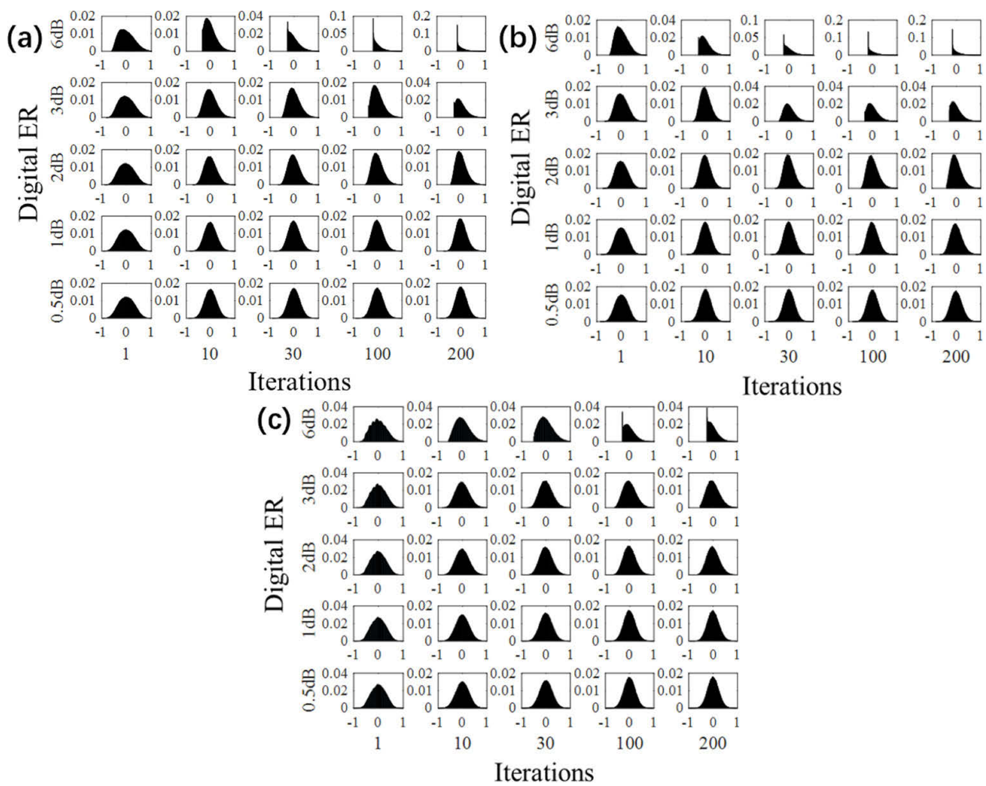

Fig. 15. (a) Transmitted amplitude distribution after pre-EDC: (a) for 28 GBaud NRZ-OOK over 100 km SMF; (b) for 56 GBaud NRZ-OOK over 50 km SMF; (c) for 28 GBaud PAM-4 over 40 km SMF.

4. Conclusion

In this paper, we successfully verify the iterative pre-electronic dispersion compensation (pre-EDC) algorithm with experimental results in IM/DD system. Three demonstrations were performed: a 28 GBaud NRZ-OOK over 100 km SMF transmission, a 56 GBaud NRZ-OOK over 50 km SMF transmission and a 28 GBaud PAM-4 over 40 km SMF transmission. The received end employed a low-complexity linear fractionally-spaced ($T/2$) post-feed-forward equalizer

Optics EXPRESS

(post-FFE). The effects of digital extinction ratio (ER), number of the pre-EDC iterations, number of the post-FFE taps and raised cosine filter roll-off factor (RoF) are investigated for these three scenarios. Results with pre-EDC show, at around −21 dBm, −15 dBm and −14 dBm received optical power (ROP) for the 28 GBaud NRZ-OOK (2 dB digital ER, 15 pre-EDC iterations and 5-tap post-FFE), 56 GBaud NRZ-OOK (1 dB digital ER, 30 pre-EDC iterations and 15-tap post-FFE) and 28 GBaud PAM-4 (2 dB digital ER, 10 pre-EDC iterations and 25-tap post-FFE) can achieve the FEC threshold of 3.8×10^{-3} BER, respectively. The presence of the pre-EDC is essential for the BER to remain lower than the FEC threshold. All these results show the practical potential of the pre-EDC employed in high-speed IM/DD systems.

Funding. National Key Research and Development Program of China (2018YFB1801701); National Natural Science Foundation of China (U1701661); Hong Kong Government (PolyU 15220120).

Disclosures. The authors declare no conflicts of interest.

Data availability. Data underlying the results presented in this paper are not publicly available at this time but may be obtained from the authors upon reasonable request.

References

1. IEEE P802.3bs 200 Gb/s and 400 Gb/s Ethernet Task Force. Available online: www.ieee802.org/3/bs/ (accessed on 20 July 2019).
2. X. Pang, O. Ozolins, S. Gaiarin, M. I. Olmedo, R. Schatz, U. Westergren, D. Zibar, S. Popov, and G. Jacobsen, "Evaluation of High-Speed EML-based IM/DD links with PAM Modulations and Low-Complexity Equalization," in *ECOC 2016; 42nd European Conference on Optical Communication*, (2016), pp. 1–3.
3. K. Zhong, X. Zhou, J. Huo, C. Yu, C. Lu, and A. P. T. Lau, "Digital Signal Processing for Short-Reach Optical Communications: A Review of Current Technologies and Future Trends," J. Lightwave Technol. **36**(2), 377–400 (2018).
4. C. Laperle and M. O'Sullivan, "Advances in High-Speed DACs, ADCs, and DSP for Optical Coherent Transceivers," J. Lightwave Technol. **32**(4), 629–643 (2014).
5. K. Schuh, F. Buchali, W. Idler, Q. Hu, W. Templ, A. Bielik, L. Altenhain, H. Langenhagen, J. Rupeter, U. Duemler, T. Ellermeyer, R. Schmid, and M. Moeller, "100 GSa/s BiCMOS DAC Supporting 400 Gb/s Dual Channel Transmission," in *ECOC 2016; 42nd European Conference on Optical Communication*, (2016), pp. 1–3.
6. H. Hettrich, R. Schmid, L. Altenhain, J. Würtele, and M. Möller, "A linear active combiner enabling an interleaved 200 GS/s DAC with 44 GHz analog bandwidth," in *2017 IEEE Bipolar/BiCMOS Circuits and Technology Meeting (BCTM)*, (2017), pp. 142–145.
7. J. C. Cartledge and A. S. Karar, "100 Gb/s Intensity Modulation and Direct Detection," J. Lightwave Technol. **32**(16), 2809–2814 (2014).
8. Q. Hu, D. Che, Y. Wang, and W. Shieh, "Advanced modulation formats for high-performance short-reach optical interconnects," Opt. Express **23**(3), 3245–3259 (2015).
9. H. Zhou, Y. Li, Y. Liu, L. Yue, C. Gao, W. Li, J. Qiu, H. Guo, X. Hong, Y. Zuo, and J. Wu, "Recent Advances in Equalization Technologies for Short-Reach Optical Links Based on PAM4 Modulation: A Review," Appl. Sci. **9**(11), 2342 (2019).
10. K. Zhong, X. Zhou, T. Gui, L. Tao, Y. Gao, W. Chen, J. Man, L. Zeng, A. P. T. Lau, and C. Lu, "Experimental study of PAM-4, CAP-16, and DMT for 100 Gb/s Short Reach Optical Transmission Systems," Opt. Express **23**(2), 1176–1189 (2015).
11. K. Zhang, Q. Zhuge, H. Xin, W. Hu, and D. V. Plant, "Performance comparison of DML, EML and MZM in dispersion-unmanaged short reach transmissions with digital signal processing," Opt. Express **26**(26), 34288–34304 (2018).
12. A. S. Karar, J. C. Cartledge, J. Harley, and K. Roberts, "Electronic Pre-Compensation for a 10.7-Gb/s System Employing a Directly Modulated Laser," J. Lightwave Technol. **29**(13), 2069–2076 (2011).
13. A. S. Karar and J. C. Cartledge, "Electronic Post-Compensation of Dispersion for DML Systems Using SCM and Direct Detection," IEEE Photonics Technol. Lett. **25**(9), 825–828 (2013).
14. N. Stojanovic, F. Karinou, Z. Qiang, and C. Prodaniuc, "Volterra and Wiener Equalizers for Short-Reach 100G PAM-4 Applications," J. Lightwave Technol. **35**(21), 4583–4594 (2017).
15. S. V. D. Heide, N. Eiselt, H. Griesser, J. J. Vegas Olmos, I. Tafur Monroy, and C. Okonkwo, "Experimental Investigation of Impulse Response Shortening for Low-Complexity MLSE of a 112-Gbit/s PAM-4 Transceiver," in *ECOC 2016; 42nd European Conference on Optical Communication*, (2016), pp. 1–3.
16. S.-R. Moon, H.-S. Kang, H. Y. Rha, and J. K. Lee, "C-band PAM-4 signal transmission using soft-output MLSE and LDPC code," Opt. Express **27**(1), 110–120 (2019).
17. J. Zhou, H. Wang, L. Liu, C. Yu, Y. Feng, S. Gao, W. Liu, and Z. Li, "C-band 56 Gbit/s on/off keying system over a 100 km dispersion-uncompensated link using only receiver-side digital signal processing," Opt. Lett. **45**(3), 758–761 (2020).

18. W. A. Ling and I. Lyubomirsky, “Electronic dispersion compensation in a 50 Gb/s optically unamplified direct-detection receiver enabled by vestigial-sideband orthogonal frequency division multiplexing,” Opt. Express **22**(6), 6984–6995 (2014).
19. P. Li, L. Yi, L. Xue, and W. Hu, “100Gbps IM/DD Transmission over 25km SSMF using 20G-class DML and PIN Enabled by Machine Learning,” in *Optical Fiber Communication Conference*, (Optical Society of America, 2018), p. W2A.46.
20. G. Goeger, C. Prodaniuc, Y. Ye, and Q. Zhang, “Transmission of intensity modulation-direct detection signals far beyond the dispersion limit enabled by phase-retrieval,” in *2015 European Conference on Optical Communication (ECOC)*, (2015), pp. 1–3.
21. G. Goeger, “Applications of Phase Retrieval in High Bit-Rate Direct-Detection Systems,” in *Optical Fiber Communication Conference*, (Optical Society of America, 2016), p. Th2A.40.
22. A. S. Karar, “Iterative Algorithm for Electronic Dispersion Compensation in IM/DD Systems,” J. Lightwave Technol. **38**(4), 698–704 (2020).
23. R. W. Gerchberg, “A practical algorithm for the determination of phase from image and diffraction plane pictures,” Optik **35**, 237–246 (1972).
24. M. Hacker, G. Stobrawa, and T. Feurer, “Iterative Fourier transform algorithm for phase-only pulse shaping,” Opt. Express **9**(4), 191–199 (2001).
25. A. Rundquist, A. Efimov, and D. H. Reitze, “Pulse shaping with the Gerchberg–Saxton algorithm,” J. Opt. Soc. Am. B **19**(10), 2468–2478 (2002).
26. T. Jannson, “Real-time Fourier transformation in dispersive optical fibers,” Opt. Lett. **8**(4), 232–234 (1983).
27. B. Kolner, “Space-time duality and the theory of temporal imaging,” IEEE J. Quantum Electron. **30**(8), 1951–1963 (1994).
28. J. Wang and K. Petermann, “Small signal analysis for dispersive optical fiber communication systems,” J. Lightwave Technol. **10**(1), 96–100 (1992).
29. F. Wyrowski, “Diffractive optical elements: iterative calculation of quantized, blazed phase structures,” J. Opt. Soc. Am. A **7**(6), 961–969 (1990).